Photocatalytic H_2 production by ethanol photodehydrogenation: Effect of anatase/brookite nanocomposites composition

Ismael Romero Ocaña [a], Alessandro Beltram [a], Juan Josè Delgado Jaén [b], Gianpiero Adami [a], Tiziano Montini [a,*], Paolo Fornasiero [a]

[a] Department of Chemical and Pharmaceutical Sciences, ICCOM-CNR, Consortium INSTM, University of Trieste, via L. Giorgieri 1, 34127 Trieste, Italy
[b] Departamento de Ciencia de los Materiales e Ingeniería Metalúrgica y Química Inorgánica, Facultad de Ciencias, Universidad de Cádiz, Campus Río San Pedro, 11510 Puerto Real, Cádiz, Spain

ARTICLE INFO

Accepted 13 January 2015

Keywords:
Photocatalytic hydrogen production
Brookite
Anatase
Titania
Photodehydrogenation

ABSTRACT

In view of the sustainable H_2 production, development of more efficient catalysts for photocatalytic reforming of oxygenated compounds is required. In this study, we report the preparation of TiO_2 nanocomposite with anatase/brookite composition prepared by hydrothermal treatments of Na-titanate precursor. The anatase/brookite ratio can be modulated changing the synthetic parameters, i.e. precursor/water mass-to volume ratio and hydrothermal treatment duration. The obtained materials present well crystallized particles with polyhedral morphology. The anatase/brookite ratio in the nanocomposite affects the mean size of Pt nanoparticles grown by photodeposition and the photocatalytic activity in H_2 production by photodehydrogenation of ethanol, with multiphasic materials presenting smaller Pt nanoparticles and higher H_2 production. The present anatase/brookite nanocomposites show higher H_2 production normalized to the surface area with respect a reference TiO_2 prepared by conventional sol–gel synthesis, suggesting that the present materials might expose a higher fraction of highly reactive facets instead of the most thermodynamically stable.

1. Introduction

Hydrogen has been widely suggested as a promising energy vector that could contribute to the replacement of a significant fraction of the fossil fuels [1–3], even if in a complex scenario that foresee a large pool of renewable biofuels [4]. Moreover, the large amount of H_2 required by the chemical industry to produce ammonia and fertilizers or to perform hydrodesulfurization (HDS), hydrodenitrogenation (HDN) and hydrogenation processes is nowadays mostly produced from fossil feedstocks, mainly by steam reforming of methane [5–7]. It is therefore mandatory to develop sustainable ways of hydrogen production. Among them, one of the most interesting medium-long term technologies is the photocatalytic reforming of aqueous solutions containing oxygenate compounds derived from biomasses [8,9]. This approach combines various positive aspects, such as sustainability of the primary energy source (the solar light), the renewability of the starting feedstock and the possible production of by-products with a high added value [8]. In addition, the easier oxidation pathway of the oxygenates molecules with respect to the more challenging water molecule makes the process more favorable, even if less sustainable with respect to the dreaming pure water splitting.

Titanium dioxide is the most investigated photocatalyst for H_2 production since it is nontoxic, relatively cheap, widely available and have an excellent stability under the reaction conditions [10,11]. Unfortunately, the bare TiO_2 work only under UV irradiation (band-gap = 3.0–3.2 eV) and presents a relatively fast electron–hole recombination rate. An increase of the TiO_2 photoresponse under visible light has been obtained by doping with metal [12–21] and non-metal elements [22–30] that can reduce the band gap or introduce intra band gap states [31]. Alternatively, some photoactivity was observed in the visible range after coupling TiO_2 with other semiconductors [32–36] or plasmonic metal nanoparticles [37–39]. The presence of metal nanoparticles can significantly increase the lifetime of the photogenerated electron–hole pairs [40–43]. This effect strongly depends on the type of TiO_2 polymorphs [44]. In fact, multiphasic TiO_2 materials demonstrated higher performances with respect to the correspondent monophasic systems in many photocatalytic processes, such as abatement and mineralization of pollutant compounds [16,24,45] or H_2 production by photoreforming/pho-

* Corresponding author.
E-mail address: tmontini@units.it (T. Montini).

todehydrogenation [46,47]. In this context, the use of composite materials comprising brookite is particularly interesting, since this polymorph is much less investigated with respect to anatase and rutile, although it demonstrated promising performances in photocatalytic applications [36,48,49]. Nowadays, a careful control of the material morphology at nanoscale level can significantly contribute to the understanding of the reactivity and bust the reactivity by exposing preferentially more reactive facets [50–54]. This approach has been widely applied to the anatase phase allowing its preparation in many different shapes [50–53,55–58]. Examples of the preparation of brookite and rutile with a controlled morphology are significantly less frequent in the literature [49,59–65]. Generally speaking, the production of preferential facets can be achieved by the addition of adequate controlling agents that adsorb on specific facets during the hydrothermal treatments employed in the preparation of anatase TiO_2 [51,52,58]. The adsorption of different controlling agents, such as F^- or Cl^-, modify the relative stability of the different facets and their growth rate, finally altering the ratio of the exposed facets and the shape of the obtained nanocrystals [52]. The obtainment of TiO_2 nanocrystals with controlled morphology favors the electron–hole separation since electrons and holes are accumulated on different facets [56,62,66]. Inspired from the synthesis of anatase nanorods reported by Li et al. [57], we prepared anatase/brookite nanocomposites by hydrothermal treatment performed under different conditions, i.e. by changing the precursor/water ratio, the heating method and the reaction time. The characterization of the obtained materials allowed us to correlate the parameters employed during the synthesis with the morphological and structural characteristics and the photocatalytic performances in hydrogen production.

2. Experimental

2.1. Synthesis of the photocatalysts

In this work, anatase/brookite nanocomposites were synthesized from Na-titanate adapting the procedure reported by Li et al. for the preparation of anatase nanorods [57].

Briefly, the Na-titanate precursor was synthesized by hydrothermal treatment of the commercial Degussa P25 TiO_2 (750 mg) at 120 °C for 24 h in a 45 mL Teflon-lined autoclave containing a NaOH 10 M solution (30 mL). The white precipitate was collected by centrifugation, washed several times with bidistilled water until the solution pH decreases below 11 and subsequently dried at 80 °C overnight.

Anatase/brookite nanocomposites were then synthesized by hydrothermal transformation of the dry Na-titanate precursor. Specifically, a 45 mL Teflon-lined autoclave was charged with 30 mL of bidistilled water and a selected amount of Na-titanate, magnetically stirring for 1 h. The hydrothermal process was performed putting the autoclave into a pre-heated oven at 200 °C for the desired time. The effect of the following parameter on the synthesis was studied: (i) the Na-titanate/water mass-to-volume ratio employed (adjusting the amount of dry Na-titanate), (ii) the heating method and (iii) the reaction time. In order to change the heating method, two different ovens were employed: a laboratory oven heating the autoclave by convection or a furnace heating the autoclave by irradiation. The conditions employed to synthesize the different samples are summarized in Table 1. After the hydrothermal treatment, the white precipitate was collected by centrifugation, washed several times with deionized water to remove the Na^+ and finally dried at 60 °C overnight. These materials were then used for the characterization and the photocatalytic tests.

Table 1
Synthesis conditions of prepared samples.

Sample	Na-titanate/water mass-to-volume ratio (mg/mL)	Time (h)	Heating method
A1	3.8	24	Convection
A2	7.7	24	Convection
A3	13.9	24	Convection
B1	3.8	24	Irradiation
B2*	7.7	24	Irradiation
B3	13.9	24	Irradiation
C1	7.7	12	Irradiation
C2	7.7	18	Irradiation
C3*	7.7	24	Irradiation
C4	7.7	30	Irradiation
C5	7.7	36	Irradiation
C6	7.7	42	Irradiation
C7	7.7	48	Irradiation

* B2 and C3 are the same sample.

A reference sol–gel TiO_2 was prepared accordingly to Gombac et al. [24]. Briefly, TiO_2-SG was prepared by hydrolysis of titanium butoxide in ethanol using HNO_3 as catalyst [24]. The gel was aged at room temperature for 24 h, dried at 80 °C overnight and finally calcined in air at 450 °C for 6 h.

0.2 wt% of Pt was loaded over these materials by photodeposition during the first photocatalytic catalytic test (see Section 2.3 for details).

2.2. Characterization techniques

X-ray diffraction (XRD) patterns were collected by a Philips X'Pert diffractometer using a Cu Kα ($\lambda = 0.154$ nm) X-ray source in the range $10° < 2\theta < 100°$ and data were analyzed by using the PowderCell 2.0 software. Mean crystallite sizes were calculated applying the Scherrer's equation to the principal reflection of each phase [(1 0 1) for anatase and (2 1 0) for brookite].

The morphology of the composite materials and the distribution of the supported Pt nanoparticles were evaluated by High Resolution Transmission Electron Microscopy (HR-TEM) and High Angle Annular Dark Field-Scanning Transmission Electron Microscopy (HAADF-STEM) images recorded by a JEOL 2010-FEG microscope operating at the acceleration voltage of 200 kV. The microscope has 0.19 nm spatial resolution at Scherzer defocus conditions in HR-TEM mode and a probe of 0.5 nm was used in HAADF-STEM mode.

Raman spectra were recorded with a Renishaw inVia microspectrometer equipped with a Nd:YAG laser using an excitation wavelength of 532 nm. The samples were dispersed onto a Si wafer and analyzed using a laser power of 1 mW in the range $100 < cm^{-1} < 1500$.

Kr physisorption at the liquid nitrogen temperature using a Micromeritics ASAP 2020 automatic analyser. The samples were previously degassed under vacuum at 120 °C for 12 h. The surface area was calculated applying the Brunauer-Emmett-Teller (BET) equation to the physisorption isotherm in the range $0.1 < p/p^0 < 0.34$.

2.3. Catalytic activity

Photocatalytic hydrogen production was studied using a Teflon-lined flow-photoreactor irradiated with a Lot-Oriel Solar Simulator equipped with a 150 W Xe lamp and an Atmospheric Edge Filter with a cut-off at 300 nm [47]. 50 mg of dried TiO_2 powder were suspended into EtOH 96% (80 mL) and 20 μL of an aqueous solution of $Pt(NO_3)_2$ (5 mg Pt mL^{-1}) were added in order to obtain a final

metal loading of 0.2 wt%. The system was purged with Ar for 30 min to remove the air before switching-on the lamp. During the photocatalytic experiments, the reactor was continuously flushed with Ar (15 mL min^{-1}) to transfer the volatile products to the analytical apparatus. All the experiments were performed maintaining the reactor temperature at 25 °C using a thermostatic bath. The incident irradiance, measured by a Delta Ohm HD 2302.0 LightMeter radiometer, was 25 mW cm^{-2} in the UV-A and 180 mW cm^{-2} in the Vis–NIR range, respectively.

On-line detection of the products in the Ar flow was carried out by an Agilent 7890A Gas Chromatograph equipped with two analytical lines. A 10 way-two loops injection valve was employed for injection during on-line analysis of the gaseous products. A Carboxen 1010 PLOT (Supelco, 30 m × 0.53 mm ID, 30 μm film) column followed by a Thermal Conductivity Detector (TCD) was used for hydrogen quantification using Ar as carrier. A DB-225 ms column (J&W, 60 m × 0.32 mm ID, 20 μm film) using He as carrier followed by a mass spectrometer (MS) HP 5975C was employed for the detection of the volatile organic compounds. The liquid phase after photocatalytic activity was collected by filtration on a 0.45 μm PVDF Millipore membrane and analyzed by GC/MS using 1-butanol as internal standard.

3. Results and discussion

3.1. Structural and textural characterization: XRD and physisorption analysis

The structure of the synthesized materials was investigated by means of powder XRD and microRaman spectroscopy. The XRD pattern of the Na-titanate precursor obtained after the hydrothermal treatment of Degussa P25 in NaOH 10 M (data not shown) presents weak and broad reflections which indicates the formation of nanocrystalline $Na_2Ti_2O_5$. Notably, the presence of considerable amounts of amorphous material cannot be excluded. Zhao et al. [67] reported the formation of $Na_2Ti_2O_5$ and $Na_2Ti_3O_7$ by hydrolysis and hydrothermal treatment at 180 °C for 24 h of $Ti(nBuO)_4$ in NaOH 6 M and 10 M, respectively. Considering that in this work TiO_2 has reacted with NaOH at a lower temperature (120 °C), it is reasonable to expect that a higher NaOH concentration is required to obtain the $Na_2Ti_2O_5$.

The XRD patterns of the products obtained after the various hydrothermal transformation of $Na_2Ti_2O_5$ are presented in Fig. 1. All the samples present well defined and resolved reflections related to anatase and brookite polymorphs, indicating a high degree of crystallization. No reflections of the Na-titanate precursor and of the rutile phase were detected: the possible presence of un-reacted $Na_2Ti_2O_5$ is hardly detected by XRD considering the amorphous/nanocrystalline nature of this material while the formation of rutile phase is usually observed during hydrolysis/hydrothermal treatments at lower pH values [67]. The phase composition (obtained by the Rietveld analysis of the XRD patterns) and the mean crystallite sizes of each phase are summarized in Table 2.

Independently on the heating method, the XRD data obtained from both A- and B-series indicate that the amount of the brookite phase and its average crystallite size increase as the Na-titanate/water ratio increases. Expanding the hydrothermal time from 12 to 24–30 h (C-series), it is possible to observe an increase in the amount of the brookite phase and a decrease of its crystallites size. Longer hydrothermal times cause a slight decrease in the content of brookite, with an increase of its mean crystallite size. Vice versa, the mean crystallite size of the anatase phase is only marginally influenced by the heating method, the Na-titanate/water ratio or the hydrothermal time.

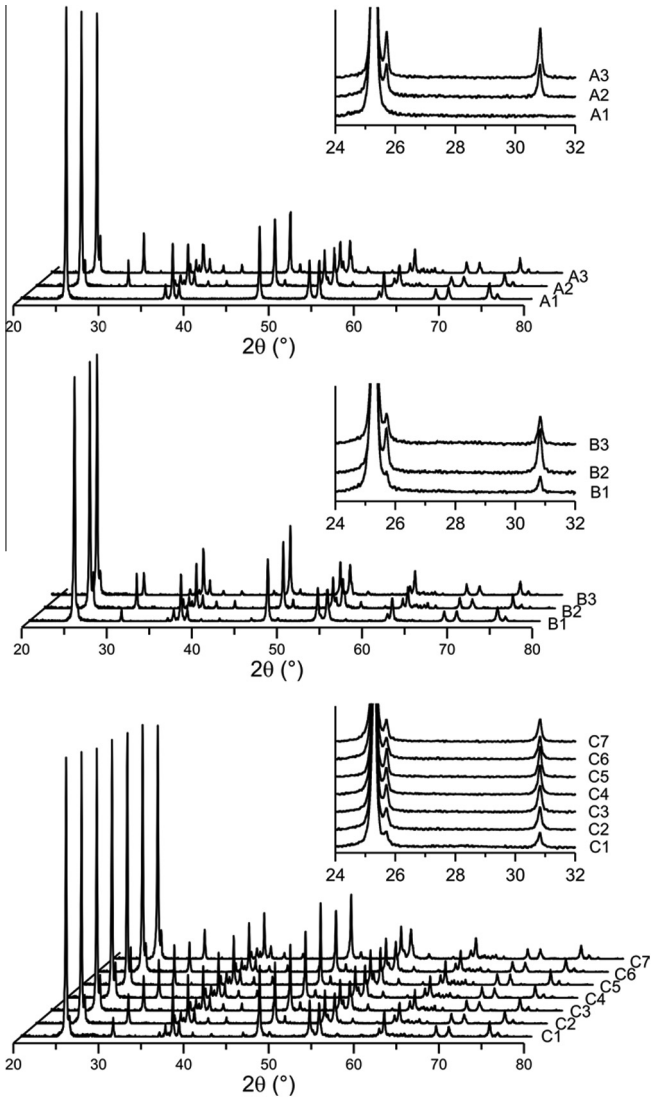

Fig. 1. Powder XRD pattern of all the prepared samples. Insets show magnification of the region where the major reflections of brookite are present, in order to appreciate the evolution of the brookite content.

Table 2
Results from XRD analysis and Kr physisorption.

	Phase composition (%)		Average crystallite size (nm)		Surface area ($m^2 g^{-1}$)
	Anatase	Brookite	Anatase	Brookite	
A1	100	–	61	–	7.2
A2	83	17	55	120	6.2
A3	73	27	72	117	8.5
B1	92	8	50	64	10.3
B2	69	31	64	89	5.7
B3	73	28	63	155	8.4
C1	88	12	61	253	74.4
C2	75	25	64	107	21.5
C3	69	31	64	89	5.7
C4	68	32	65	77	5.2
C5	71	29	66	85	6.1
C6	74	26	62	143	4.9
C7	77	23	63	275	5.0

The Raman spectra (Fig. 2), which are sensitive also to the presence of small amount of amorphous surface phases, further confirm the trends observed by means of the XRD measurements.

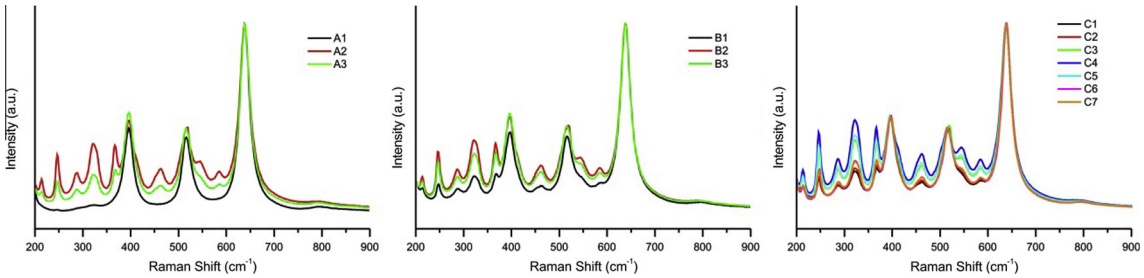

Fig. 2. Raman spectra of all the prepared samples. The anatase band at 143 cm^{-1} is omitted for clarity. Spectra are normalized with respect to the intensity of the anatase band at 639 cm^{-1}.

The presence of anatase can be revealed by the bands at 143, 195, 395, 515 and 639 cm^{-1} while the bands at 213, 245, 282, 320, 365, 456, 502, 545 and 584 cm^{-1} are characteristic of brookite [46]. All the collected spectra are dominated by the very intense band of anatase at 143 cm^{-1}, which has been removed from the spectra of Fig. 2 to better appreciate the contribution of the less intense bands of the brookite.

The BET surface area of the anatase/brookite composites are summarized in Table 2. Notably, the $Na_2Ti_2O_5$ precursor used for the synthesis of these materials presents a relatively high surface area of 84 $m^2\ g^{-1}$. Vice-versa, despite the different anatase/brookite composition, the surface area of the samples in the A- and B-series are always very low (5–10 $m^2\ g^{-1}$). The samples of the C-series show that the surface area of the materials decreases during the first 24 h of reaction, settling below 10 $m^2\ g^{-1}$ for longer hydrothermal treatments. These data suggest that the most important modifications in the composite take place during the first 24 h of the hydrothermal conversion of the Na titanate into TiO_2.

The observed evolution in anatase/brookite composition can be interpreted on the base of the transformation that the $Na_2Ti_2O_5$ precursor undergoes during the hydrothermal treatment as proposed in Scheme 1.

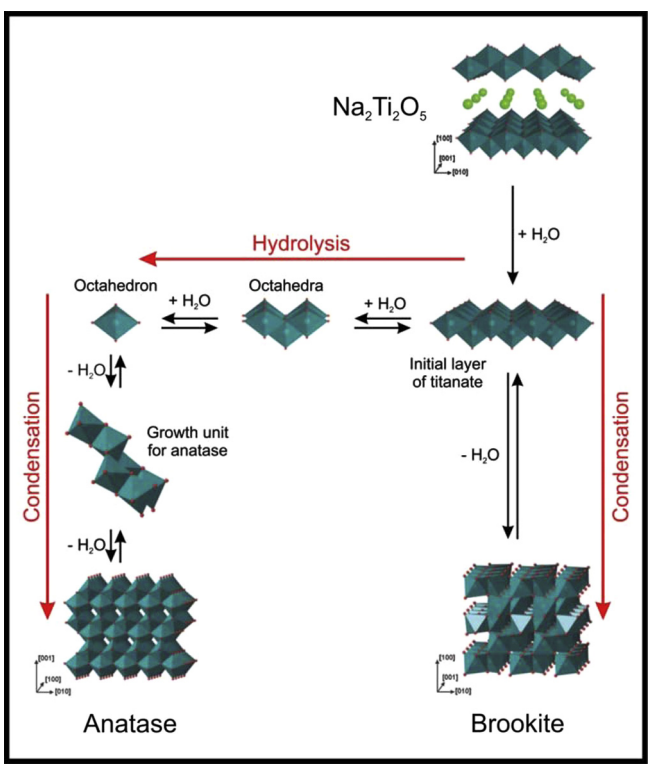

Scheme 1. Proposed transformations taking place during the hydrothermal treatment of $Na_2Ti_2O_5$.

The Na-titanate precursor consists of negatively charged layers made of TiO_6 octahedrons linked through the edges and spaced by Na^+ ions. In the first step of the transformation, the exfoliation of the layers takes place releasing NaOH and increasing the pH of the solution as the hydrothermal treatment proceeds. Condensation of the exfoliated layers through the octahedrons vertices leads to formation of the brookite phase following the "Ostwald's step rule" [67,68]: in fact, brookite is the phase having the most similar structure and, therefore, the nearest free energy compared to the precursor (the exfoliated titanate layers). On the other hand, the formation of anatase requires the complete hydrolysis in the TiO_6 octahedrons and their subsequent condensation since, in the anatase phase, the octahedrons are linked through the edges. In this case, the transformation of the Na-titanate follows the Ostwald's ripening, providing the most stable product.

The data of the C-series suggest that, during the first 24 h of the hydrothermal treatment, $Na_2Ti_2O_5$ is preferentially converted into anatase. After 12 h of reaction, the pH of the solution is around 11, ideal conditions for the slow growth of brookite forming large crystallites. As the hydrothermal treatment proceeds, more NaOH is released in solution increasing the pH and further favoring the formation of the brookite phase, in agreement with the results reported by Zhao et al. [67]. Notably, TEM data and surface area measures indicate that the conversion of $Na_2Ti_2O_5$ is complete only after 24 h of reaction. The maximum amount of brookite is obtained for the samples recovered after 24–30 h of hydrothermal treatment. In these samples, the mean crystallite sizes of brookite is rather small, in agreement with the fast formation of the brookite phase. After longer treatments, the slightly increase in the anatase content indicates that brookite is slowly converted into anatase through hydrolysis and re-condensation. Although rutile is known as the thermodynamically stable TiO_2 polymorph, the relative stability of brookite and anatase still remains an open topic. The data obtained in this study suggest that anatase is more stable than brookite at least under the employed synthetic conditions (high pH, temperature, presence of Na^+). In fact, it is reasonable that the relative stability of the two metastable polymorphs depends on numerous factors, including the crystallite size, the exposed faces and the presence of adsorbates on the surface [50]. Moreover, the increase in the mean crystallite size of brookite for hydrothermal treatments longer than 24 h suggests that the brookite nanocrystals with the smallest dimensions are involved in the re-dissolution, leading to the growth of larger brookite crystallites and/or to their partial hydrolysis and conversion into anatase.

3.2. Morphological characterization: TEM studies

The catalysts were collected after the photocatalytic tests in order to morphologically characterize both the TiO_2 substrate and the photodeposited Pt nanoparticles. To this purpose, both a HR-TEM and HAADF-STEM techniques were employed.

The morphology of the TiO_2 substrates were analyzed in order to evidence the possible effects of the preparation conditions on it. All samples present a high crystallinity degree and large particle size, in agreement with the well defined XRD reflections, the mean crystallite sizes calculated from XRD analysis and the low surface areas. In the anatase/brookite nanocomposites, two different kinds of TiO_2 particles can be observed: polycrystalline elongated particles and polycrystalline and polyhedral clusters. The ratio of the two structures changes depending on phase composition of the materials. Fig. 3 shows representative images of selected samples prepared under different hydrothermal conditions. The sample A1, prepared using the lower titanate/water ratio, presents only polycrystalline elongated particles that have an average crystallite size in excellent agreement with the size measured by XRD. Notably, adopting similar preparation conditions, Li et al. [57] reported the preparation of anatase nanorods formed by single crystalline particles. Although pure anatase was obtained also in our case, the polycrystalline nature of the sample A1 can be ascribed to the slightly different experimental conditions. Increasing the titanate/water ratio, some polycrystalline and polyhedral clusters (100 nm–1.5 μm) appear in the sample A2, becoming preponderant in the sample with the higher titanate/water ratio (sample A3). All the samples of the B-series present polycrystalline and polyhedral clusters (100 nm – 1 μm) independently of the titanate/water ratio employed. The EDX analysis of the samples of the series A and B did not detect significant amounts of sodium (EDS spectrum in Fig. 3), as a possible residue of the Na-titanate precursor. With the aim to clearly attribute the crystallographic phase to the different types of observed nanoparticles by TEM, Digital Diffraction Patterns (DDP) have been analyzed. Unfortunately, only in a limited number of cases, the particles have been univocally identified as anatase or brookite by the comparison of the experimental DDP with the theoretical diffraction patterns of both phases and considering different axis zones. In the most part of the analyzed DDP, reasonable fits with features typical of both the phases were possible, probably because of the overlapping of crystallites in the nanocomposite material and the similar spacing present in both phases. Due to this, a clear relationship between the different morphologies observed and the crystal phases cannot be defined.

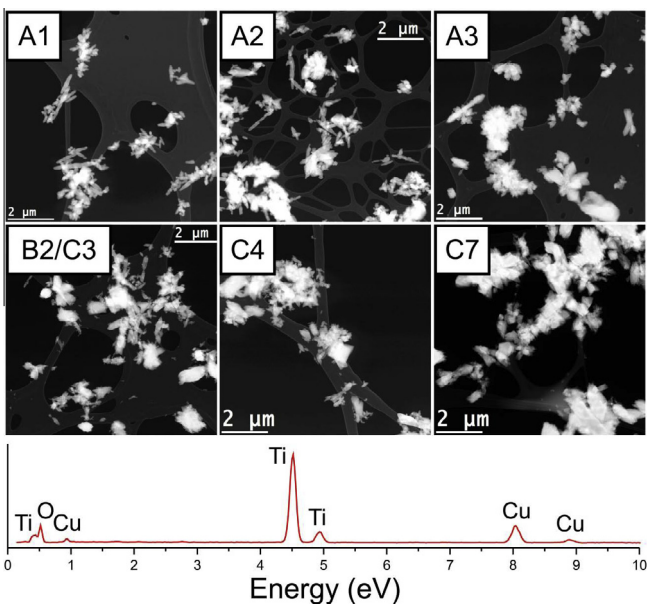

Fig. 3. Representative HAADF-STEM images of selected samples to highlight the evolution of the morphology of the TiO_2 nanocomposite materials. A typical EDX spectrum taken on the well-defined nanocrystals shows the absence of clear peaks related to Na.

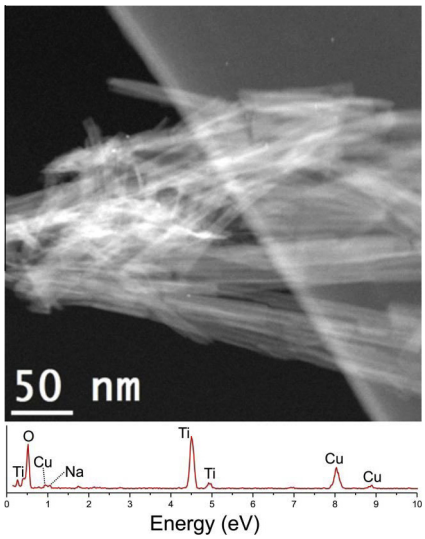

Fig. 4. Image of a selected portion of the sample C1, evidencing the presence of nanotube morphology. The EDX spectrum taken in this area shows an amount of Na significantly higher than in the rest on the material (see Fig. 3).

Analyzing the samples of the C-series, an interesting morphological change from the Na-titanate to the anatase/brookite composites was observed due to the different time of hydrothermal treatment. Samples C1 and C2 (12 and 18 h of hydrothermal treatment) clearly show the presence of particles with nanotube morphology (see Fig. 4). The EDX analysis performed on these structures show the presence of a considerable amount of Na, significantly higher with respect to the other portions of the samples. Similar structures were reported in several works as the result of NaOH-based hydrothermal treatment of TiO_2 [69–72]. Therefore, this peculiar structures can be reasonably related to the Na-titanate precursor unconverted during the hydrothermal treatment. Consistently a higher surface area is observed for the samples C1 and C2. Notably, in the samples hydrothermally treated for more than 24 h, particles with nanotube morphology were not observed, evidencing the presence only of polycrystalline and polyhedral clusters (100 nm – 2 μm). Moreover, the EDX analysis performed on the samples C3 – C7 reveals a significantly lower amounts of Na or its absence (below detection limits). These results confirm that the Na-titanate needs more than 24 h to be completely converted into TiO_2.

The HR-TEM analysis of the samples evidence the presence of a large number of Pt nanoparticles deposited on the surface of the TiO_2 substrates. The Pt nanoparticles over the TiO_2 surface are single crystals, as suggested by the presence of the lattice fringes in HR-TEM analysis (see Fig. 5).

Fig. 6 shows some representative HAADF-STEM images of the dispersion of Pt nanoparticles on the surface of the TiO_2 support. Analyzing the position of the Pt nanoparticles detectable as bright spots in Fig. 6, it is possible to observe that they are concentrated on particular regions of the samples. In fact, TiO_2 particles homogenously covered by Pt nanoparticles have been observed together with other TiO_2 particles on which Pt nanoparticles are almost absent (i.e., samples A1, A3, C4). Moreover, in some cases, Pt nanoparticles concentrated on grain boundaries and/or on corners of the TiO_2 crystals have been observed (i.e., samples B2/C3 and C1). Considering that electrons are necessary to reduce Pt ions and to grow the metal nanoparticles, the position of Pt nanoparticles can be used to identify the regions of the photoactive TiO_2

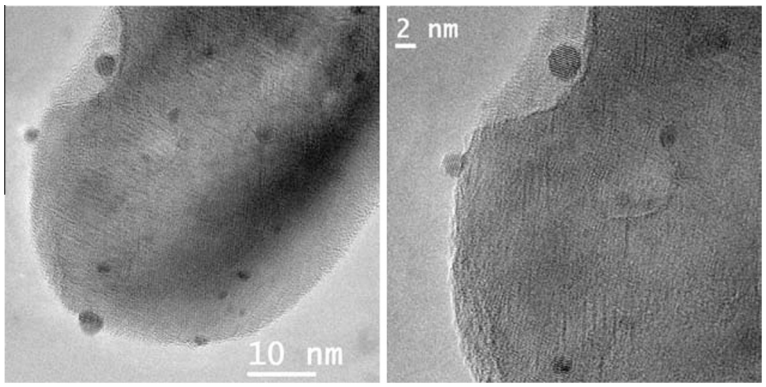

Fig. 5. Representative HR-TEM images showing the crystalline nature of the Pt nanoparticles.

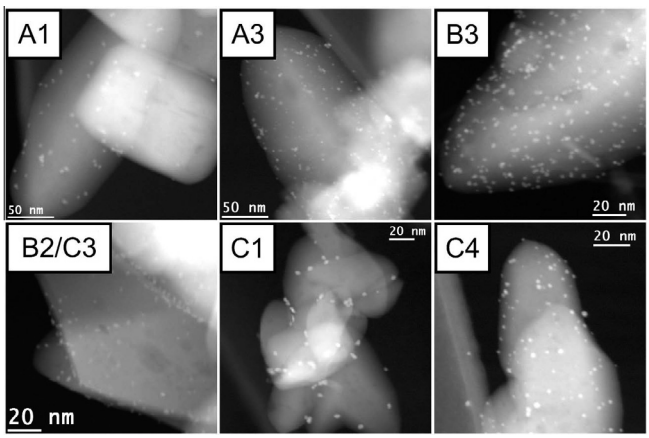

Fig. 6. Representative HAADF-STEM images collected on selected samples, showing the Pt nanoparticles after photodeposition on the TiO_2 supports.

support where electrons are preferentially accumulated [62,73]. The distribution of the Pt nanoparticles on the surface of the anatase/brookite prepared in this work suggests that the morphological and structural characteristics on the supports favor a deep electron–hole separation thanks to the well-defined surfaces.

The analysis of the size distribution of the Pt nanoparticles is summarized in Fig. 7. Small Pt nanoparticles, with mean size of 2.0 – 2.5 nm, were observed for the samples prepared using a TiO_2 support composed by a mixture of anatase and brookite. Conversely, larger Pt nanoparticles, with mean size of 4 – 6 nm, were observed in the samples presenting low or zero brookite content (samples A1, A2) or residual Na-titanate (samples C1, C2). This is in agreement with the fact that the junctions between crystallites of different TiO_2 phases favor the electron–hole separation after irradiation of the semiconductor material, increasing the number of nucleation sites on which Pt ions can be reduced and Pt nanoparticles can growth. Similarly, Cu nanoparticles prepared by photodeposition on a polycrystalline TiO_2 support present a smaller mean size with respect to those grown on pure anatase [47].

3.3. Functional characterization: H_2 production by ethanol photodehydrogenation

The photocatalytic activity of the synthesized anatase/brookite nanocomposites was evaluated studying the sustainable H_2 production from ethanol aqueous solution under irradiation with simulated sunlight. Commercial azeotropic ethanol/water solutions (containing ~96% by volume of ethanol) was used as feedstock to avoid changing in the composition during photocatalytic experiments due to selective evaporation in the inert gas flow. Preliminary experiments performed on the A1 sample revealed that the H_2 production using EtOH 96% is comparable to that obtained using EtOH/H_2O 50/50 mixture [19,47,74], while it is significantly higher than the H_2 obtained using pure EtOH. These results indicate that a very low amount of water is sufficient to effectively promote the photocatalytic production of H_2 using EtOH as sacrificial agent, in agreement with previous studies on the dependence of H_2 productivity on the composition of EtOH/H_2O solutions [75,76]. Blank experiments were performed without irradiation and no H_2 evolution was observed.

The on-line analysis of the volatile products revealed that H_2 was the major product in the gas stream, together with minor amounts of acetaldehyde and 1,1-diethoxyethane. Any other by-products, such as CH_4, CO_2, CO or ethylene, were observed. Irre-

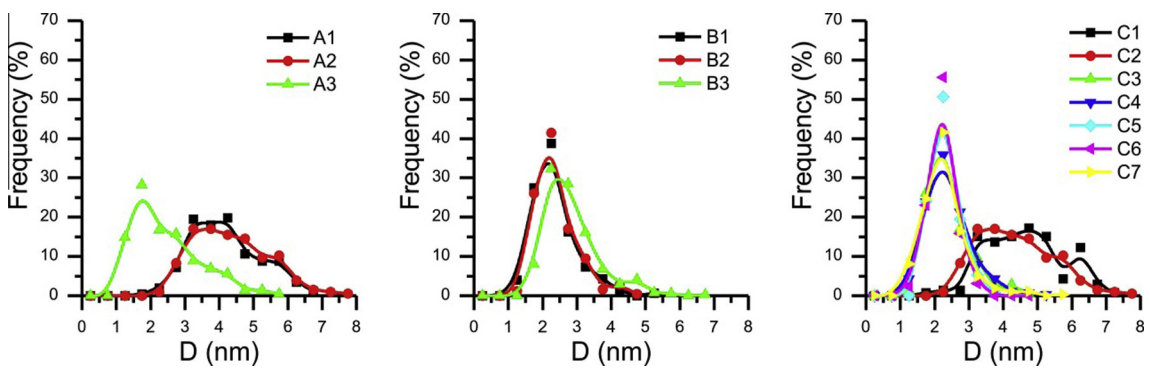

Fig. 7. Size distribution of the Pt nanoparticles for the synthesised samples.

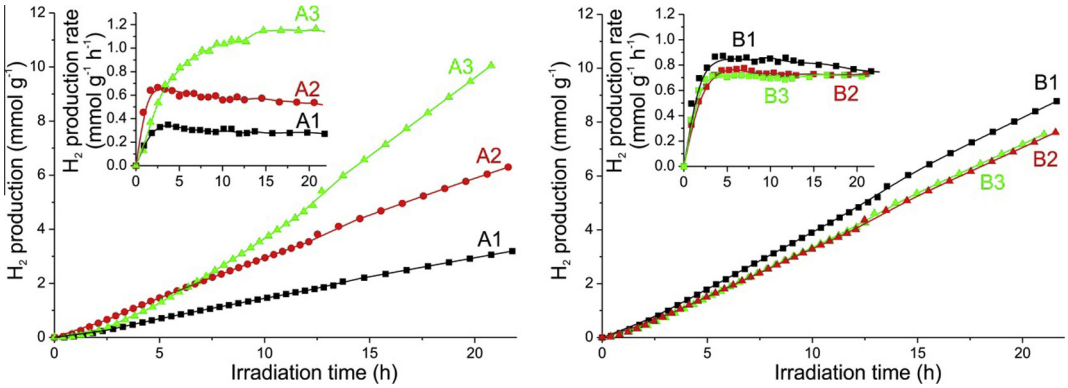

Fig. 8. H_2 evolution during ethanol photodehydrogenation under simulated sunlight irradiation of the catalysts of the A- and B-series. The insets show the H_2 production rates.

spectively from the different activities demonstrated by the samples (see below), the analysis of the liquid phases, collected at the end of the photocatalytic experiments, evidenced the presence of acetaldehyde and 1,1-diethoxyethane, accordingly to the results of the on-line analysis. Heaviest products, such as 2,3-butanediol, were not detected, in agreement with the fact that these products are formed when highly energetic UV photons are used for the irradiation [77].

Fig. 8 presents the H_2 evolution for the samples of the A- and B-series as a function of the irradiation time. It evidences that the heating method for the hydrothermal conversion of Na-titanate precursor into TiO_2 nanocomposite plays an important role to drive the final photocatalytic performances. For all the samples, the H_2 production rate progressively increases during the first 4 – 5 h in concomitance with the occurrence of photodeposition of Pt nanoparticles on the surface of the TiO_2. After this activation period, the observed activities remain constant for all the materials, without appreciable deactivation. The obtained results evidenced that the hydrogen production rate significantly enhances for samples of the A-series as the Na-titanate/water ratio increases whereas it is only marginally influenced by the irradiation heating method (B-series).

Fig. 9 shows the H_2 production for the samples of the C-series, prepared by varying only the hydrothermal reaction time. As already observed, the H_2 production rate increases during the first 4 – 6 h due to the occurrence of the concomitant deposition of the Pt nanoparticles. The photocatalytic H_2 production increases as the time of hydrothermal treatment increases up 30 h while, for longer reaction times, no significant changes were observed. This is an indication that the completeness of the Na-titanate/TiO_2 transformation is necessary to obtain a high photocatalytic activity in the photodehydrogenation of ethanol, although the surface area of the photoactive material is significantly reduced. A photocatalytic activity experiment performed using bare Na-titanate showed an H_2 production rate that is ~ 10 time lower than that obtained using the anatase/brookite nanocomposites produced by hydrothermal treatment longer than 24 h (samples C4 – C7).

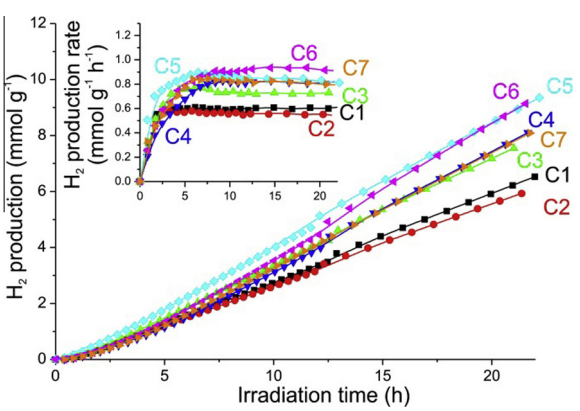

Fig. 9. H_2 evolution during ethanol photodehydrogenation under simulated sunlight using the catalysts of the C-series. The inset shows the H_2 production rates.

To better understand these results, it is necessary to focus on the mechanism of the ethanol photoreforming. In a mixture of ethanol and water, the stoichiometric reaction for H_2 photoreforming is:

$$CH_3CH_2OH + 3H_2O \rightarrow 6H_2 + 2CO_2 \quad (1)$$

In our case, the complete oxidation of ethanol is not achieved since CO_2 evolution is not observed during the photocatalysis. Therefore, the main process is the photocatalytic dehydrogenation of the ethanol leading to acetaldehyde and H_2. Due to the low adsorption capability of acetaldehyde and to the high concentration of ethanol, subsequent oxidation of acetaldehyde is highly unfavorable. The oxidation mechanism of ethanol over TiO_2 surface starts with the formation of surface ethoxide and OH groups by dissociative adsorption on the surface of TiO_2 [8]. This process competes with H_2O adsorption. The photooxidation process involves the direct electron transfer from the ethoxide to photogenerated holes of TiO_2 meanwhile hydrogen of OH groups are reduced by photogenerated electrons trapped in the Pt nanoparticles. The produced acetaldehyde could be further oxidized to acetic acid if adsorbed on the surface or in solution by free $OH^{\cdot}$ radical. Otherwise acetaldehyde is accumulated in solution providing a less volatile compound. The high concentration of 1,1-diethoxyethane found in the liquid phase confirms that acetaldehyde react with ethanol.

In the literature it is well reported that the nanocomposite of different TiO_2 polymorphs are more active than the single phases both in oxidation [78,79] and in reduction [46,47,80–82] processes due to the formation of heterojunctions between the crystallites of the different phases and the capability of photogenerated electrons and holes to transfer from phase to phase. Kandiel et al. [83] reported that flatband potential and quasi-Fermi level of brookite nanorods and of brookite/anatase nanocomposites are shifted to a more negative potential with respect to pure anatase. This reflects in a higher driving force for proton reduction in brookite-containing materials, favoring interfacial electron transfer while the resulting energy barrier would suppress back electron transfer [83].

Fig. 10 clearly demonstrates that the sample containing both brookite and anatase phases are significantly more active than

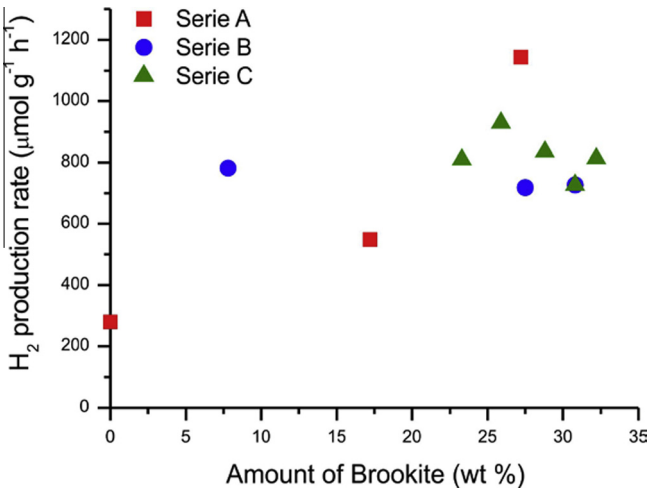

Fig. 10. Stationary H_2 production rates as a function of brookite content in the studied materials. Samples C1 and C2 are omitted since the brookite content is warped by the amount of unconverted Na-titanate precursor, hardly detected by XRD.

the sample containing only anatase. The heating method mainly influence the amount of brookite and, accordingly, the activity of the materials. On the other hand, there is no relations between the amount of brookite and the activity of the samples prepared via irradiation heating.

The obtained results suggest that the photocatalytic activity of the Pt-anatase/brookite nanocomposites studied in this work cannot be simply correlated with the structural properties but requires to fully involve also morphological aspects, and in particular the surface area and the exposed faces of each sample. In particular, the most important differences observed between the A- and B-series could be ascribed to potential different interaction/contact between the anatase and brookite crystallites, as a result of the different heating method adopted during the synthesis.

To better understand the relative influence of these parameters, it is necessary to compare the present performances with those of a well-known reference TiO_2-based material. To this aim, we considered a TiO_2 obtained by sol–gel after hydrolysis of Ti(*i*-PrO)$_4$ in a solution of H_2O and HNO_3 in ethanol [47,84]. After calcination at 420 °C for 6 h, the XRD pattern of this material presents anatase (64%), brookite (28%) and rutile (8%) phases and a surface area of 69 $m^2\ g^{-1}$. After photodeposition of 0.2 wt% Pt, Pt nanoparticles

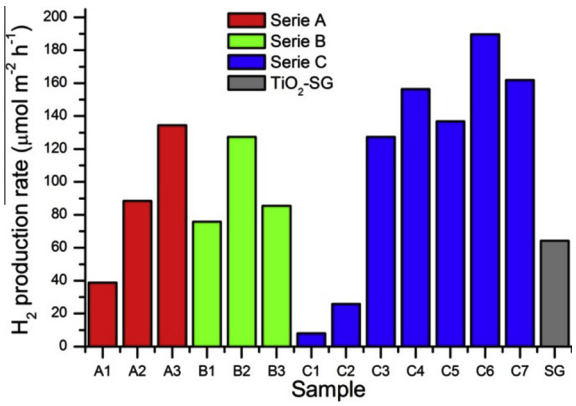

Fig. 11. H_2 production during EtOH photodehydrogenation of a suspension of the prepared samples and the TiO_2 prepared via sol–gel (TiO_2-SG), normalized per surface area.

of about 2.5 nm were obtained as confirmed by means HAADF-STEM. The photocatalytic hydrogen production of this material, normalized per gram of catalyst, is significantly higher with respect to those obtained here. However, normalizing the performances on the bases of the surface area of the samples (Fig. 11), the materials prepared in this study shows interesting/superior performance. Notably, the normalization by surface area is significant as the ethanol photodehydrogenation requires ethanol adsorption on the surface.

This result suggests that the hydrothermal treatment used for the preparation of the samples studied allows the crystals to grow exposing crystallographic facets that are more actives than the facets exposed by the TiO_2 prepared via sol–gel. This material is synthesized in the absence of template agents and is subsequently calcined, so it is reasonable to assume that it exposes the more thermodynamically stable facets instead of the more actives. This important aspect requires further investigation, and will be the subject of a more in depth HR-TEM investigation.

4. Conclusions

In this study, anatase/brookite nanocomposite were prepared by hydrothermal treatment of Na-titanate precursor. The composition can be tuned by changing the Na-titanate/water mass-to-volume ratio and the duration of the hydrothermal treatment, as confirmed by XRD and Raman analysis. Under the adopted conditions, a hydrothermal treatment longer than 24 h is required for the complete conversion of the $Na_2Ti_2O_5$ precursor into TiO_2 materials. The products are well crystallized materials with polyhedral and polycrystalline morphologies, resulting in quite low surface area (lower than 10 $m^2\ g^{-1}$). The size distribution of Pt nanoparticles prepared by photodeposition is strongly influenced by the anatase/brookite ratio. Larger Pt nanoparticles (> 4 nm) were observed in the samples with incomplete conversion of the $Na_2Ti_2O_5$ precursor and/or with the lower amounts of brookite. High H_2 photocatalytic production rates were observed for samples with multiphasic anatase/brookite supports and small Pt nanoparticles (∼ 2 nm). These results are related with the favored electron/hole separation obtained with the use of multiphasic TiO_2 materials. Comparing the activity of these materials prepared by hydrothermal treatment with that of a reference TiO_2 prepared by conventional sol–gel followed by calcination in air, the present anatase/brookite nanocomposites showed a higher H_2 production normalized to the surface area. This indicates that the present anatase/brookite nanocomposites expose the more reactive facets. Future developments of this work include the modification of the hydrothermal conditions by addition of templating and/or directing agents to control the growth of the particles with the aim to reduce the crystallite size of anatase and brookite phases and improve the specific surface area.

Acknowledgements

Universities of Trieste (Italy) and Cadiz (Spain), ICCOM-CNR, Consortium INSTM, Regione Lombardia for project Atlante, FP7-NMP-2012-SMALL-6 (project ID 310651), HI-PHUTURE (protocol 2010N3T9M4) and COST Action CM1104 are acknowledged for financial support. J.J.D.J. would like to thank the contribution of the Ramon y Cajal program.

References

[1] C.C. Elam, C.E. Gregoire Padró, G. Sandrock, A. Luzzi, P. Lindblad, E. Fiermestad Hagen, Int. J. Hydrogen Energy 28 (2003) 601.
[2] S. Dunn, Int. J. Hydrogen Energy 27 (2002) 235.
[3] M. Momirlan, T. Veziroglu, Int. J. Hydrogen Energy 30 (2005) 795.

[4] S. Zinoviev, F. Müller-Langer, P. Das, N. Bertero, P. Fornasiero, M. Kaltschmitt, G. Centi, S. Miertus, ChemSusChem 3 (2010) 1106.
[5] R. Ramachandran, R.K. Menon, Int. J. Hydrogen Energy 23 (1998) 593.
[6] R.M. Navarro, M.A. Peña, J.L.G. Fierro, Chem. Rev. 107 (2007) 3952.
[7] J.D. Holladay, J. Hu, D.L. King, Y. Wang, Catal. Today 139 (2009) 244.
[8] M. Cargnello, A. Gasparotto, V. Gombac, T. Montini, D. Barreca, P. Fornasiero, Eur. J. Inorg. Chem. 2011 (2011) 4309.
[9] D.I. Kondarides, A. Patsoura, X.E. Verykios, (n.d.).
[10] T. Inoue, A. Fujishima, S. Konishi, K. Honda, Nature (1979) 277.
[11] G. Palmisano, V. Augugliaro, M. Pagliaro, L. Palmisano, Chem. Commun. (Camb.) (2007) 3425.
[12] T. Umebayashi, T. Yamaki, H. Itoh, K. Asai, J. Phys. Chem. Solids 63 (2002) 1909.
[13] D. Dvoranová, V. Brezová, M. Mazúr, M.A. Malati, Appl. Catal. B Environ. 37 (2002) 91.
[14] K. Wilke, H.D. Breuer, J. Photochem. Photobiol. A Chem. 121 (1999) 49.
[15] H. Yamashita, Y. Ichihashi, M. Takeuchi, S. Kishiguchi, M. Anpo, J. Synchrotron Radiat. 6 (1999) 451.
[16] A. Di Paola, E. García-López, S. Ikeda, G. Marcı, B. Ohtani, L. Palmisano, Catal. Today 75 (2002) 87.
[17] J. Choi, H. Park, M.R. Hoffmann, J. Phys. Chem. C 114 (2010) 783.
[18] A. Naldoni, M. Allieta, S. Santangelo, M. Marelli, F. Fabbri, S. Cappelli, C.L. Bianchi, R. Psaro, V. Dal, J. Am. Chem. Soc. 134 (2012) 7600.
[19] A. Gallo, T. Montini, M. Marelli, A. Minguzzi, V. Gombac, R. Psaro, P. Fornasiero, V. Dal, ChemSusChem 5 (2012) 1800.
[20] W.H. Saputera, G. Mul, M.S. Hamdy, Catal. Today (2014).
[21] M.S. Hamdy, R. Amrollahi, G. Mul, ACS Catal. 2 (2012) 2641.
[22] G. Liu, C. Sun, S.C. Smith, L. Wang, G.Q.M. Lu, H.-M. Cheng, J. Colloid Interface Sci. 349 (2010) 477.
[23] G. Liu, H.G. Yang, X. Wang, L. Cheng, J. Pan, G.Q.M. Lu, H.-M. Cheng, J. Am. Chem. Soc. 131 (2009) 12868.
[24] V. Gombac, L. De Rogatis, A. Gasparotto, G. Vicario, T. Montini, D. Barreca, G. Balducci, P. Fornasiero, E. Tondello, M. Graziani, Chem. Phys. 339 (2007) 111.
[25] M. Fittipaldi, V. Gombac, A. Gasparotto, C. Deiana, G. Adami, D. Barreca, T. Montini, G. Martra, D. Gatteschi, P. Fornasiero, ChemPhysChem 12 (2011) 2221.
[26] M. Bettinelli, V. Dallacasa, D. Falcomer, P. Fornasiero, V. Gombac, T. Montini, L. Romanò, A. Speghini, J. Hazard. Mater. 146 (2007) 529.
[27] G. Liu, Y. Zhao, C. Sun, F. Li, G.Q. Lu, H.-M. Cheng, Angew. Chem., Int. Ed. Engl. 47 (2008) 4516.
[28] S.U.M. Khan, M. Al-Shahry, W.B. Ingler, Science 297 (2002) 2243.
[29] L. Lin, W. Lin, Y. Zhu, B. Zhao, Y. Xie, Chem. Lett. 34 (2005) 284.
[30] M.V. Dozzi, E. Selli, J. Photochem. Photobiol. C. Photochem. Rev. 14 (2013) 13.
[31] C. Di Valentin, G. Pacchioni, Catal. Today 206 (2013) 12.
[32] Y. Zhu, Z. Chen, T. Gao, Q. Huang, F. Niu, L. Qin, P. Tang, Y. Huang, Z. Sha, Y. Wang, Appl. Catal. B Environ. 163 (2015) 16.
[33] I. Robel, M. Kuno, P.V. Kamat, J. Am. Chem. Soc. 129 (2007) 4136.
[34] Y. Ma, R. Chong, F. Zhang, Q. Xu, S. Shen, H. Han, C. Li, Phys. Chem. Chem. Phys. 16 (2014) 17734.
[35] C. Wang, R.L. Thompson, J. Baltrus, C. Matranga, J. Phys. Chem. Lett. 1 (2010) 48.
[36] M. Guo, L. Li, H. Lin, Y. Zuo, X. Huang, G. Li, Chem. Commun. (Camb). 49 (2013) 11752.
[37] W. Chen, Y. Lu, W. Dong, Z. Chen, M. Shen, Mater. Res. Bull. 50 (2014) 31.
[38] J. Li, H. Zhou, S. Qian, Z. Liu, J. Feng, P. Jin, X. Liu, Appl. Phys. Lett. 104 (2014) 261110.
[39] J.S. DuChene, B.C. Sweeny, A.C. Johnston-Peck, D. Su, E.A. Stach, W.D. Wei, Angew. Chem., Int. Ed. Engl. 53 (2014) 7887.
[40] R. Baba, S. Nakabayashi, A. Fujishima, K. Honda, J. Phys. Chem. 89 (1985) 1902.
[41] V. Subramanian, E. Wolf, P.V. Kamat, J. Phys. Chem. B 105 (2001) 11439.
[42] V. Subramanian, E.E. Wolf, P.V. Kamat, J. Am. Chem. Soc. 126 (2004) 4943.
[43] A.W. Maijenburg, J. Veerbeek, R. de Putter, S.A. Veldhuis, M.G.C. Zoontjes, G. Mul, J.M. Montero-Moreno, K. Nielsch, H. Schäfer, M. Steinhart, J.E. ten Elshof, J. Mater. Chem. A 2 (2014) 2648.
[44] T. Luttrell, S. Halpegamage, J. Tao, A. Kramer, E. Sutter, M. Batzill, Sci. Rep. 4 (2014) 4043.
[45] B. Zhao, F. Chen, Y. Jiao, H. Yang, J. Zhang, J. Mol. Catal. A Chem. 348 (2011) 114.
[46] Y. Liu, Z. Wang, W. Wang, W. Huang, J. Catal. 310 (2014) 16.
[47] T. Montini, V. Gombac, L. Sordelli, J.J. Delgado, X. Chen, G. Adami, P. Fornasiero, ChemCatChem 3 (2011) 574.
[48] B. Zhao, F. Chen, Q. Huang, J. Zhang, Chem. Commun. (Camb). (2009) 5115.
[49] L. Zhang, V.M. Menendez-Flores, N. Murakami, T. Ohno, Appl. Surf. Sci. 258 (2012) 5803.
[50] T.R. Gordon, M. Cargnello, T. Paik, F. Mangolini, R.T. Weber, P. Fornasiero, C.B. Murray, J. Am. Chem. Soc. 134 (2012) 6751.
[51] C. Liu, X. Han, S. Xie, Q. Kuang, X. Wang, M. Jin, Z. Xie, L. Zheng, Chem. Asian J. 8 (2013) 282.
[52] L. Wu, B.X. Yang, X.H. Yang, Z.G. Chen, Z. Li, H.J. Zhao, X.Q. Gong, H.G. Yang, CrystEngComm 15 (2013) 3252.
[53] G. Liu, J.C. Yu, G.Q. Lu, H.-M. Cheng, Chem. Commun. 47 (2011) 6763.
[54] M. Cargnello, B.T. Diroll, Nanoscale 6 (2014) 97.
[55] J. Pan, G. Liu, G.Q.M. Lu, H.-M. Cheng, Angew. Chem., Int. Ed. Engl. 50 (2011) 2133.
[56] N. Roy, Y. Sohn, D. Pradhan, ACS Nano 7 (2013) 2532.
[57] J. Li, D. Xu, Chem. Commun. 46 (2010) 2301.
[58] H.G. Yang, C.H. Sun, S.Z. Qiao, J. Zou, G. Liu, S.C. Smith, H.M. Cheng, G.Q. Lu, Nature 453 (2008) 638.
[59] G. Zhu, T. Lin, X. Lü, W. Zhao, C. Yang, Z. Wang, H. Yin, Z. Liu, F. Huang, J. Lin, J. Mater. Chem. A 1 (2013) 9650.
[60] R. Buonsanti, V. Grillo, E. Carlino, C. Giannini, T. Kipp, R. Cingolani, P.D. Cozzoli, J. Am. Chem. Soc. 130 (2008) 11223.
[61] K. Kakiuchi, E. Hosono, H. Imai, T. Kimura, S. Fujihara, J. Cryst. Growth 293 (2006) 541.
[62] T. Ohno, K. Sarukawa, M. Matsumura, New J. Chem. 26 (2002) 1167.
[63] H. Zhao, L. Liu, J.M. Andino, Y. Li, J. Mater. Chem. A 1 (2013) 8209.
[64] B. Liu, E.S. Aydil, J. Am. Chem. Soc. 131 (2009) 3985.
[65] C. Xiong, X. Deng, J. Li, Appl. Catal. B Environ. 94 (2010) 234.
[66] X. Ma, Y. Dai, M. Guo, B. Huang, Langmuir 29 (2013) 13647.
[67] B. Zhao, L. Lin, D. He, J. Mater. Chem. A 1 (2013) 1659.
[68] R.A. Van Santen, J. Phys. Chem. 88 (1984) 5768.
[69] Y. Mao, S.S. Wong, J. Am. Chem. Soc. 128 (2006) 8217.
[70] X. Sun, Y. Li, Chemistry 9 (2003) 2229.
[71] D.V. Bavykin, J.M. Friedrich, F.C. Walsh, Adv. Mater. 18 (2006) 2807.
[72] C.-C. Tsai, H. Teng, Chem. Mater. 18 (2006) 367.
[73] T. Ohno, T. Higo, N. Murakami, H. Saito, Q. Zhang, Y. Yang, T. Tsubota, Appl. Catal. B Environ. 152–153 (2014) 309.
[74] V. Gombac, L. Sordelli, T. Montini, J.J. Delgado, A. Adamski, G. Adami, M. Cargnello, S. Bernal, P. Fornasiero, J. Phys. Chem. A 114 (2010) 3916.
[75] N. Strataki, V. Bekiari, D.I. Kondarides, P. Lianos, Appl. Catal. B Environ. 77 (2007) 184.
[76] D.I. Kondarides, V.M. Daskalaki, A. Patsoura, X.E. Verykios, Catal. Lett. 122 (2007) 26.
[77] A. Gasparotto, D. Barreca, D. Bekermann, A. Devi, R.A. Fischer, P. Fornasiero, V. Gombac, O.I. Lebedev, C. Maccato, T. Montini, G. Van Tendeloo, E. Tondello, J. Am. Chem. Soc. 133 (2011) 19362.
[78] C.A. Emilio, M.I. Litter, M. Kunst, M. Bouchard, C. Colbeau-Justin, Langmuir 22 (2006) 3606.
[79] J.T. Carneiro, T.J. Savenije, J.A. Moulijn, G. Mul, J. Phys. Chem. C 115 (2011) 2211.
[80] C.-H. Lin, C.-H. Lee, J.-H. Chao, C.-Y. Kuo, Y.-C. Cheng, W.-N. Huang, H.-W. Chang, Y.-M. Huang, M.-K. Shih, Catal. Lett. 98 (2004) 61.
[81] H.-L. Kuo, C.-Y. Kuo, C.-H. Liu, J.-H. Chao, C.-H. Lin, Catal. Lett. 113 (2007) 7.
[82] C.-H. Lin, J.-H. Chao, C.-H. Liu, J.-C. Chang, F.-C. Wang, Langmuir 24 (2008) 9907.
[83] T.A. Kandiel, A. Feldhoff, L. Robben, R. Dillert, D.W. Bahnemann, Chem. Mater. 22 (2010) 2050.
[84] H. Zhang, J.F. Banfield, J. Phys. Chem. B 104 (2000) 3481.